

# Electronic structure of $(\text{GaAs})_m(\text{AlAs})_n$ superlattices grown in the $[211]$ direction

Z. Ikonc, G. P. Srivastava, and J. C. Inkson

*Department of Physics, Exeter University, Stocker Road, Exeter EX4 4QL, United Kingdom*

(Received 30 January 1995; revised manuscript received 25 April 1995)

The electronic structure of  $(\text{GaAs})_m(\text{AlAs})_n$  superlattices, with  $2 \leq (m, n) \leq 13$ , grown in the  $[211]$  direction is calculated by the local empirical pseudopotential method within the  $S$ -matrix implementation. The calculated results are discussed and compared to those for other growth directions.

Superlattices have traditionally been grown along high-symmetry directions, mainly  $[001]$ , and sometimes  $[110]$  and  $[111]$ . Recently, however, experimental and theoretical studies of other growth directions have also appeared, e.g., for  $[113]$ ,<sup>1-3</sup>  $[211]$ ,<sup>4,5</sup> and others. These higher-index growth directions are considered interesting for a number of applications. They enable an optimization of the normal-incidence intersubband transitions for infrared photodetectors,<sup>6,7</sup> and offer some advantages over the conventional growth directions when used in semiconductor lasers. They also may provide a means for the fabrication of quantum-wire structures. Note, however, that while high-index growth usually results in corrugated interfaces leading to quantum-wire formation, it is also possible to grow essentially perfect flat-interface superlattices.<sup>1</sup>

There have been relatively few detailed theoretical studies of the electronic band structure of higher-index superlattices. Most of the calculations of the conduction-band states in quantum wells grown in the  $[211]$  direction (and also some others) have been made within the effective-mass approximation.<sup>6,7</sup> Application of this method is acceptable for the thicker structures that may be used in photodetectors, but it is not so reliable for thin period superlattices. In this paper we present the electronic band structure of  $[211]$ -grown GaAs/AlAs superlattices at all the important Brillouin-zone points where low-energy structure is to be expected, calculated within the  $S$ -matrix and empirical pseudopotential frameworks. To our knowledge there have been no other microscopic calculations for this growth direction.

The details of the technique we used are described in our previous papers.<sup>8,9</sup> Briefly, the complex band structures of the bulk semiconductors, which are the constituents of the superlattice, are first calculated using the local empirical pseudopotential theory. These are then used to calculate the wave-function propagation across the superlattice period, which is implemented via the  $S$ -matrix formalism to ensure high stability against evanescent states. Once the superlattice period  $S$  matrix is found, it is recast into the transfer  $T$  matrix, and the Bloch theorem applied. Both short as well as long superlattice periods may be treated in this way, without encountering any computational problems.<sup>9</sup> Various states in the superlattice Brillouin zone are accessed by presetting an appropriate value of the in-plane projection ( $\mathbf{k}_\parallel$ ) of electron wave vec-

tor, within the interface Brillouin zone. The third wave-vector component, along the superlattice axis, arises from the calculation.

The  $(211)$  interface Brillouin zone is given in Fig. 1. The interface Brillouin zone is a good indicator of groups of bulk states that might undergo mixing in a superlattice electronic state. The most relevant points are the symmetry points in the irreducible segment  $\bar{\Gamma}$ ,  $\bar{X}$ ,  $\bar{M}$ , and  $\bar{N}$ , which have projected or folded onto them the most important bulk Brillouin-zone points  $\Gamma$ ,  $X$ , and  $L$ . Specifically, the  $\Gamma$  and one pair of  $X$  points project into  $\bar{\Gamma}$ , while the other four  $X$  points project into the two equivalent  $\bar{X}$  points. Four  $L$  points project into the two  $\bar{M}$ , and the other four into four  $\bar{N}$  points. Therefore the low-energy conduction-band superlattice states are expected to be found at the  $\bar{\Gamma}$ ,  $\bar{X}$ ,  $\bar{M}$ , and  $\bar{N}$  points. We should note that the inequivalence of, say,  $\bar{M}$  and  $\bar{N}$  points can be seen as follows. The angles between the superlattice axis and the principal ellipsoidal axes of  $L$  valleys projected into the  $\bar{M}$  point are  $19.5^\circ$  (or  $160.6^\circ$ ) and  $90^\circ$ , and for the valleys projected into the  $\bar{N}$  point they amount to  $61.9^\circ$  ( $118.1^\circ$ ). It follows therefore that the  $L$ -derived electronic (miniband) structure at  $\bar{M}$  and  $\bar{N}$  points will be different. Similarly, the corresponding angles for the  $X$ -valley ellipsoids projected into  $\bar{\Gamma}$  are  $35.3^\circ$  ( $144.7^\circ$ ), and for those projected into  $\bar{X}$  amount to  $65.9^\circ$  ( $114.1^\circ$ ), and therefore the two sets of  $X$ -derived minibands will also have different energies. There is the possibility of mixing of the  $\Gamma$  and  $X$  bulk states in  $\bar{\Gamma}$  minibands (beyond the effective-mass theory), due to their coincident folding in the interface Brillouin zone. Minibands at points other than  $\bar{\Gamma}$ , on the other hand, will be essentially single band (i.e., either  $X$  or  $L$ ) derived, with no

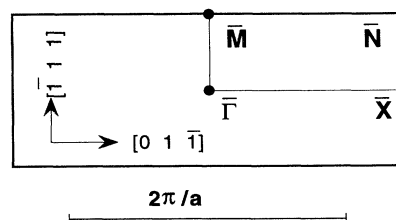


FIG. 1. The interface Brillouin zone for the  $[211]$ -oriented GaAs/AlAs superlattice. Characteristic points  $\bar{\Gamma}$ ,  $\bar{X}$ ,  $\bar{M}$ , and  $\bar{N}$ , having folded or projected onto them the bulk Brillouin-zone points,  $\Gamma$ ,  $X$ , and  $L$ , are also denoted.

significant mixing of bulk states.

Numerical calculations were performed using the pseudopotential formfactors of Ref. 10 for both GaAs and AlAs. For the wave-function propagation and matching

at interfaces, 63 two-dimensional plane waves were used, corresponding to 89 three-dimensional reciprocal-lattice vectors. The valence-band-edge discontinuity assumed in the calculations was 0.45 eV, in accordance with the ex-

TABLE I. Electron energies in  $(\text{GaAs})_m(\text{AlAs})_n$  superlattices grown in the  $[211]$  direction. For each  $(m, n)$  combination the first five lines give the lowest conduction-band states at  $\bar{\Gamma}$ ,  $\bar{X}$ ,  $\bar{M}$ , and  $\bar{N}$  interface Brillouin-zone points, and the sixth line gives the highest valence-band states at  $\bar{\Gamma}$ . The character of the conduction-band states at  $\bar{\Gamma}$  is given in brackets. All the energies are in eV units, and are measured from the conduction-band edge of GaAs. Numbers of GaAs monolayers ( $m$ ) and of AlAs monolayer ( $n$ ) in a superlattice period vary vertically and horizontally, respectively.

$m \backslash n$		2	3	4	5	6	7	8
$\bar{\Gamma}(\Gamma)$	2	0.407	0.473	0.485	0.564	0.590	0.569	0.634
$\bar{\Gamma}(X)$		0.351	0.322	0.298	0.300	0.292	0.285	0.279
$\bar{X}$		0.354	0.336	0.314	0.313	0.301	0.296	0.287
$\bar{M}$		0.377	0.413	0.422	0.453	0.466	0.475	0.483
$\bar{N}$		0.417	0.442	0.437	0.469	0.474	0.481	0.484
$\bar{\Gamma}$		-1.578	-1.627	-1.658	-1.680	-1.697	-1.709	-1.719
$\bar{\Gamma}(\Gamma)$	3	0.312	0.388	0.436	0.477	0.509	0.536	0.558
$\bar{\Gamma}(X)$		0.370	0.331	0.333	0.321	0.311	0.301	0.293
$\bar{X}$		0.381	0.345	0.345	0.321	0.321	0.303	0.304
$\bar{M}$		0.372	0.397	0.434	0.441	0.449	0.457	0.467
$\bar{N}$		0.401	0.416	0.437	0.446	0.459	0.463	0.470
$\bar{\Gamma}$		-1.534	-1.579	-1.611	-1.632	-1.648	-1.663	-1.673
$\bar{\Gamma}(\Gamma)$	4	0.242	0.320	0.368	0.402	0.444	0.468	0.488
$\bar{\Gamma}(X)$		0.383	0.369	0.352	0.338	0.326	0.316	0.307
$\bar{X}$		0.387	0.377	0.357	0.346	0.332	0.324	0.314
$\bar{M}$		0.370	0.404	0.415	0.426	0.438	0.445	0.451
$\bar{N}$		0.376	0.407	0.418	0.433	0.441	0.449	0.454
$\bar{\Gamma}$		-1.503	-1.544	-1.573	-1.594	-1.610	-1.623	-1.634
$\bar{\Gamma}(\Gamma)$	5	0.217	0.274	0.315	0.371	0.395	0.417	0.446
$\bar{\Gamma}(X)$		0.405	0.386	0.365	0.344	0.338	0.327	0.319
$\bar{X}$		0.407	0.377	0.371	0.348	0.345	0.327	0.326
$\bar{M}$		0.402	0.388	0.402	0.415	0.427	0.430	0.442
$\bar{N}$		0.385	0.393	0.409	0.419	0.431	0.436	0.445
$\bar{\Gamma}$		-1.482	-1.517	-1.544	-1.564	-1.578	-1.590	-1.598
$\bar{\Gamma}(\Gamma)$	6	0.186	0.242	0.286	0.323	0.355	0.381	0.404
$\bar{\Gamma}(X)$		0.414	0.393	0.375	0.360	0.348	0.337	0.327
$\bar{X}$		0.411	0.395	0.378	0.366	0.353	0.344	0.334
$\bar{M}$		0.367	0.384	0.396	0.408	0.417	0.425	0.431
$\bar{N}$		0.368	0.387	0.398	0.411	0.419	0.428	0.434
$\bar{\Gamma}$		-1.467	-1.497	-1.521	-1.538	-1.551	-1.562	-1.570
$\bar{\Gamma}(\Gamma)$	7	0.160	0.214	0.254	0.287	0.321	0.353	0.365
$\bar{\Gamma}(X)$		0.420	0.400	0.380	0.368	0.355	0.335	0.334
$\bar{X}$		0.422	0.393	0.387	0.366	0.362	0.344	0.342
$\bar{M}$		0.360	0.373	0.387	0.397	0.409	0.413	0.422
$\bar{N}$		0.362	0.376	0.390	0.400	0.411	0.417	0.425
$\bar{\Gamma}$		-1.454	-1.481	-1.501	-1.516	-1.529	-1.538	-1.544
$\bar{\Gamma}(\Gamma)$	8	0.147	0.193	0.228	0.265	0.293	0.315	0.338
$\bar{\Gamma}(X)$		0.425	0.402	0.384	0.374	0.361	0.350	0.339
$\bar{X}$		0.424	0.409	0.391	0.381	0.367	0.358	0.347
$\bar{M}$		0.358	0.371	0.380	0.393	0.401	0.408	0.415
$\bar{N}$		0.357	0.372	0.382	0.395	0.403	0.411	0.417
$\bar{\Gamma}$		-1.445	-1.469	-1.486	-1.498	-1.509	-1.516	-1.524

perimental data. The corresponding values of conduction-band discontinuities at  $\Gamma$ ,  $X$ , and  $L$  points were 0.842,  $-0.245$ , and  $0.215$  eV, respectively (the “ $-$ ” sign indicating that the  $X$  point is lower in AlAs). When compared to the corresponding values obtained by applying the “65/35” rule to the experimentally measured band gaps of GaAs and AlAs,<sup>11</sup> the discontinuities at  $\Gamma$  and  $X$  are about right, and the value for  $L$  is twice as large. However, *ab initio* calculations predict the discontinuity at  $L$  to be  $\sim 0.5$  eV (e.g., Ref. 12). Thus the above value appearing in our calculations lies in between the experimental and *ab initio* theoretical values. Finally, the spin-orbit coupling constants were chosen so that the split-off bands in GaAs and AlAs were 0.35 and 0.32 eV below the corresponding valence-band maxima, respectively.

The energies of the lowest conduction-band states (miniband bottoms) at  $\bar{\Gamma}$ ,  $\bar{X}$ ,  $\bar{M}$ , and  $\bar{N}$  points of the interface Brillouin zone, as well as the topmost valence miniband at  $\bar{\Gamma}$ , were calculated for all  $(\text{GaAs})_m(\text{AlAs})_n$  superlattices in the range  $2 \leq (m, n) \leq 8$ . (Actually, both the lowest  $\Gamma$ -derived and lowest  $X$ -derived minibands were found at the  $\bar{\Gamma}$  point.) The thickness of one monolayer in the  $[211]$  direction is  $a/2\sqrt{6} \approx 0.153$  nm, where  $a$  is the cubic lattice constant. Although some doubts may be cast on the reliability of the empirical pseudopotential approach when dealing with very thin layers, comprising say 2 ML (in view of the fact that this approach does not account for the charge redistribution), previous experience with  $[001]$ ,  $[110]$ , and  $[111]$  superlattices<sup>9,13</sup> indicates that results are at least qualitatively correct even for layers as thin as that.

The results of the present calculations at selected  $k_{\parallel}$  values are given in Table I. All the energies (including those of the valence-band states) are measured from the conduction-band edge of GaAs at  $\Gamma$ . The states at  $\bar{X}$ ,  $\bar{M}$ , and  $\bar{N}$  interface Brillouin-zone points are always off the center of the superlattice Brillouin zone. Therefore, when the lowest miniband bottom occurs at any of these points the superlattice is an indirect-band-gap material. The lowest-energy bulk  $\Gamma$ -derived state at the  $\bar{\Gamma}$  point always corresponds to the center of the superlattice Brillouin zone (and, if it lies absolutely lowest, makes the particular superlattice a direct-band-gap material). On the other hand, the extrema of bulk  $X$ -derived minibands at  $\bar{\Gamma}$  are at the superlattice Brillouin-zone center when  $m+n$  is even, and at Brillouin-zone edges when  $m+n$  is odd. Thus, an  $m+n$ =even superlattice with the absolutely lowest  $X$ -derived miniband at  $\bar{\Gamma}$  is a quasidirect-band-gap material. There may be some difficulty in classifying the lowest superlattice state as  $\Gamma$  or  $X$  derived if the two minibands lie at energies close to each other (and hence show strong  $\Gamma$ - $X$  mixing) at the center of the superlattice Brillouin zone. In other words, in such cases minibands cannot be reliably classified from simply knowing the relative contributions of bulk states in the superlattice state wave function. It would become necessary to investigate the dispersion of such minibands off the zone center.

An inspection of the results given in Table I reveals that the lowest conduction-band superlattice state occurs

in either the  $\bar{\Gamma}$  or  $\bar{X}$  minibands, the  $L$ -derived minibands at  $\bar{M}$  and  $\bar{N}$  points always lying higher. The  $\Gamma$ -derived miniband is the lowest for *all*  $m > n$  superlattices, giving a direct band gap, while those with  $m < n$  in the range explored have either an indirect or a quasidirect gap, as explained above. It is interesting to note a nonsmooth or even nonmonotonic (decaying oscillatory) behavior of  $X$ -derived  $\bar{\Gamma}$  or  $\bar{X}$  miniband energies as the number of AlAs monolayers increases. The same is observed for  $L$ -derived  $\bar{M}$  and  $\bar{N}$  minibands as the number of GaAs monolayers increases. These features are clearly not in accordance with the effective-mass well-barrier picture. This is due to the microscopic cell-periodic parts of the wave functions and the need to match them over the superlattice interfaces. Also worth noting is that the lowest bulk  $X$ -derived miniband at  $\bar{X}$  is slightly higher than the corresponding one at  $\bar{\Gamma}$ . In the language of effective-mass theory this is because the  $X$ -valley ellipsoids projected onto  $\bar{X}$  are somewhat more tilted than those projected onto  $\bar{\Gamma}$ , thus having a smaller effective mass in the quantization direction.

Looking at the main diagonal of Table I ( $m=n$ ), we note that the thin-period  $[211]$   $(\text{GaAs})_n(\text{AlAs})_n$  superlattices ( $n \leq 7$ ) have a quasidirect band gap, the lowest conduction-band state being the  $X$ -derived miniband at the  $\bar{\Gamma}$  point. This lowest state is rather purely  $X$  in character if  $n < 7$ , in spite of the possibility of  $\Gamma$ - $X$  mixing. For  $n=7$ , however, there is a sizable contribution from the bulk  $\Gamma$  state in the lowest superlattice state, but it is still more  $X$  derived. For  $n=8$  the  $[211]$   $(\text{GaAs})_n(\text{AlAs})_n$  superlattice becomes a direct-band-gap material, although very marginally (by 1 meV only). There is a large amount of bulk state mixing here, with the  $\Gamma$  and  $X$  bulk states making approximately equal contributions to the lowest superlattice state. As a partial extension of Table I, we also made calculations for the diagonal  $m=n=9-13$  cases. The energies of  $\Gamma$ - and  $X$ -derived miniband bottoms at  $\bar{\Gamma}$  are found to be  $E_{\Gamma}=0.340$  eV,  $E_X=0.325$  eV for  $n=9$ ;  $E_{\Gamma}=0.320$  eV,  $E_X=0.331$  eV for  $n=10$ ;  $E_{\Gamma}=0.328$  eV,  $E_X=0.310$  eV for  $n=11$ ;  $E_{\Gamma}=0.302$  eV,  $E_X=0.321$  eV for  $n=12$ ; and  $E_{\Gamma}=0.294$

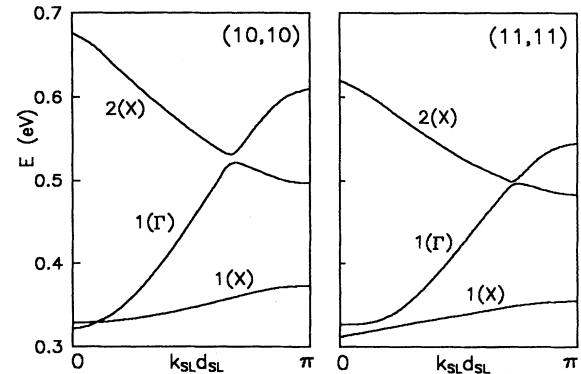


FIG. 2. The dispersion of the lowest  $\Gamma$ -derived and two lowest  $X$ -derived conduction minibands in a direct gap ( $m=n=10$ ) and a quasidirect gap ( $m=n=11$ ) GaAs/AlAs $[211]$  superlattice. The energies are measured as in Table I.

eV,  $E_X = 0.316$  eV for  $n = 13$ . Similarly to  $n = 7$  and 8, the  $n = 9-11$  cases show a high degree of  $\Gamma$ - $X$  mixing, but for  $n = 12$  and beyond the lowest superlattice state is almost purely  $\Gamma$  in character. Therefore the [211]-grown  $(\text{GaAs})_m(\text{AlAs})_n$  superlattices for  $n < 7$  have a quasidirect band gap, those with  $n > 11$  have a direct gap, and the cases  $n = 7-11$  show an oscillatory quasidirect-direct behavior, though in fact they cannot be quite unambiguously classified because of roughly even contributions of bulk  $\Gamma$  and  $X$  states to the lowest superlattice state at the center of the superlattice Brillouin zone. As for the top-most valence-band state, in all the cases it is heavy-hole-like, displaying a smooth dependence on the superlattice parameters, as expected from the well-barrier picture. In respect to the oscillatory behavior of miniband energies as the superlattice period varies, and to the changeover to direct band gap for sufficiently large  $n$ , the [211] superlattices are more similar to [001], [110], and [113] than to [111] ones (e.g., Refs. 2, 3, 9, and 13).

Examples of the band structures (conduction bands only) of direct-gap ( $m = n = 10$ ) and quasidirect-gap ( $m = n = 11$ ) superlattices are given in Fig. 2. It is interesting to note that in the former case the more dispersive  $\Gamma$ -derived miniband is intersected by two less disper-

sive  $X$ -derived minibands, but anticrossing behavior occurs only with the second  $X$  miniband. In the  $m = n = 11$  (quasidirect gap) case, the lowest  $X$  miniband is always below the  $\Gamma$ -derived one, but anticrossing behavior with the second  $X$  miniband remains.

In conclusion, the electronic band structure of [211]-grown  $(\text{GaAs})_m(\text{AlAs})_n$  superlattices was calculated within the empirical pseudopotential framework. It is found that short-period ( $n < 7$ )  $(\text{GaAs})_m(\text{AlAs})_n$  superlattices have a quasidirect band gap, with the lowest miniband being bulk  $X$  derived. The type of band gap in the superlattices with  $7 \leq m = n \leq 11$  oscillates between quasidirect (for odd  $n$ ) and direct (even  $n$ ), although this classification is somewhat ambiguous because of strong mixing of  $\Gamma$  and  $X$  bulk states in the lowest miniband superlattice states. Superlattices with  $m = n \geq 12$  are predicted to have a direct band gap. If  $m > n$ , even by a single monolayer, the band gap is always direct.

The authors would like to thank the EPSRC (UK) for computational facilities through the CSI scheme. One of the authors (Z.I.) is grateful to the EPSRC (UK) for financial support.

<sup>1</sup>Y. Hsu, W. I. Wang, and T. S. Kuan, Phys. Rev. B **50**, 4973 (1994).

<sup>2</sup>D. A. Contreras-Solorio, V. R. Velasco, and F. Garcia-Molinari, Phys. Rev. B **47**, 4651 (1993); **48**, 12 319 (1993).

<sup>3</sup>Z. Ikonik, G. P. Srivastava, and J. C. Inkson, Phys. Rev. B **49**, 10 749 (1994).

<sup>4</sup>Z. V. Popovic, E. Richter, J. Spitzer, M. Cardona, R. Notzel, and K. Ploog, Superlatt. Microstruct. **14**, 129 (1993).

<sup>5</sup>P. Castrillo, M. I. Alonso, G. Armelles, M. Ilg, and K. Ploog, Phys. Rev. B **47**, 12 945 (1993).

<sup>6</sup>H. Xie, J. Katz, and W. I. Wang, J. Appl. Phys. **72**, 3681

(1992).

<sup>7</sup>W. Xu, Y. Fu, M. Willander, and S. C. Shen, Phys. Rev. B **49**, 13 760 (1994).

<sup>8</sup>D. Y. K. Ko and J. C. Inkson, Phys. Rev. B **38**, 9945 (1988).

<sup>9</sup>Z. Ikonik, G. P. Srivastava, and J. C. Inkson, Phys. Rev. B **46**, 15 150 (1992).

<sup>10</sup>E. Caruthers and C.-L. Chung, Phys. Rev. B **17**, 2705 (1978).

<sup>11</sup>S. Adachi, J. Appl. Phys. **58**, R1 (1985).

<sup>12</sup>S. H. Wei and A. Zunger, J. Appl. Phys. **63**, 5794 (1988).

<sup>13</sup>Z. Ikonik, J. C. Inkson, and G. P. Srivastava, Semicond. Sci. Technol. **7**, 648 (1992).